Proceedings of the ASME 2011 Dynamic Systems and Control Conference
DSCC2011
October 31 - November 2, 2011, Arlington, VA, USA

DSCC2011-6177

MODEL BASED FAULT DETECTION OF FREEWAY TRAFFIC SENSORS

Gunes Dervisoglu *

Department of Mechanical Engineering
University of California
Berkeley, California 94720
Email: gunesder@berkeley.edu

Roberto Horowitz

Department of Mechanical Engineering
University of California
Berkeley, California 94720
Email: horowitz@berkeley.edu

ABSTRACT

This paper presents a model based fault detection and exclusion scheme that implements a decision logic to automatically identify faulty or mislocated freeway traffic sensors in the presence of unknown on-ramp and off-ramp flows. The algorithm is deployed within the framework of a suite of software tools, named TOPl, which models traffic flow via a macroscopic model, calibrates the model based on available data and runs simulations to evaluate various operational strategies such as ramp metering, demand management, incident management, etc. TOPl has been used to model various freeways in California, such as Interstate 80, Interstate 210, Interstate 880 and Interstate 680. Two main difficulties with data collection on California freeways were found to be missing ramp flow and faulty mainline data, which decrease the accuracy of the model and increase the time and effort invested in model calibration. The former of these difficulties has been previously addressed by an iterative learning algorithm that estimates the missing ramp flows and the latter is tackled by the method presented in this work.

1 INTRODUCTION

Software models of traffic flow provide city planners with essential tools to study the operation of traffic corridors. These models can be used to study the benefits of improvement strategies such as ramp metering and incident management. First order macroscopic models like the Cell Transmission Model (CTM) [1] are widely used to simulate traffic flow and design control strategies. The Asymmetric Cell Transmission Model (ACTM) [2] is a modified version of the CTM, which is particularly suited to modeling freeway traffic flow. The main advantage of using a first order macroscopic model, such as the ACTM, is the ease of model specification, calibration and evaluation of optimal strategies [2].

In TOPl [3], the model specification and calibration procedure for traffic corridors consists of 5 main steps: 1) Network Specification, 2) Fundamental Diagram Calibration, 3) Ramp Flow Imputation (if ramp data is missing), 4) Fault Detection and Exclusion 5) Simulation. The first step determines the geometry of the corridor to be modeled and specifies the elements (cells) of the model to be calibrated. The second step fits the empirical fundamental diagram to traffic data provided by loop detectors assigned to each cell in the model. In the third step, missing ramp flow data is estimated by an imputation scheme based on an iterative learning algorithm. The results of this imputation constitute the on-ramp and off-ramp flow inputs to the model (Steps 1-3 are explained in more detail in the next section). The imputation procedure is carried out for a given single day's data and needs to be redone for every other day, so that the measurements along the freeway are consistent with the mathematical model. However, since the imputation scheme is based on the mainline traffic data, it is highly sensitive to any fault in the loop detector measurements and erroneous data can lead to erratic ramp flows which in turn give rise to poor simulation results that do not match the measurements satisfactorily. Consequently, the fourth step of the modeling effort comprises a model based fault detection and exclusion methodology which determines which mainline loop detectors are supplying poor quality data.

The inductive loop detectors on California freeways provide occupancy and flow data. These data are stored and archived by

*Address all correspondence to this author.

PeMS [4], an online repository for traffic data with various tools and services, which also calculates and provides other essential quantities such as density and speed derived from the measured occupancies and flows. This repository has its own built-in fault detection method [5], which is based purely on detecting irregularities in the time series data that fall into one of the following four cases: 1) Zero Occupancy and Flow for an extended period, 2) Non-zero occupancy accompanied by zero flow, 3) Very high Occupancy, 4) Constant Occupancy and Flow. These four modes of failure are obvious indicators of hardware malfunction and relatively straight forward to detect and assess. Other improved statistical methods are provided in [6] and [7]. However, the main difficulty is that some detectors are found to be reporting systematically biased data, which are not possible to be picked out by statistical methods. A model based approach to address this problem is provided in [8], where the freeway flow is modeled by Hamilton-Jacobi partial differential equations and the consistency of data collected at certain locations is tested against the continuous model in the space-time domain. However, the effect of unknown inputs in the form of missing ramp flows are not taken into account by this method. A non-automated ad-hoc methodology to determine the faulty measurements in the presence of unknown ramp flows was demonstrated in [9]. Here, discarding the manually picked faulty detectors decreased the model errors of 9% in density and 15% in flow to 3% and 9% respectively. This work builds on the methodology of [9] to automate the procedure of flagging faulty detectors. Once the faulty detectors are determined, their data is excluded from the calibration procedure.

The rest of the paper is organized as follows: Section 2 presents the ACTM and summarizes the model calibration and unknown input estimation procedures, section 3 explains the model based fault detection and exclusion scheme and the automation thereof, section 4 presents the results of the methodology and section 5 provides the concluding remarks.

2 THE ASYMMETRIC CELL TRANSMISSION MODEL, CALIBRATION AND IMPUTATION

This section summarizes the ACTM and the calibration and imputation procedures based on it. The details of both procedures are given in [10] and [11], respectively. The ACTM specifies the freeway as a sequence of cells, each with at most one on-ramp near the beginning of the section and at most one off-ramp near the end of the section (see figure 1). In all figures in this paper, traffic is assumed to flow from left ro right. Every cell has a detector station associated with it, and when specifying the model geometry, it is aimed to build the cells in a such a way that every cell contains one vehicle detector station (vds). Each cell of the freeway is characterized by a fundamental diagram (Figure 2) which is an empirical curve relating observed flows and densities on a given cross-section of the road. These fundamental diagrams are calibrated using multiple days' data. [10].

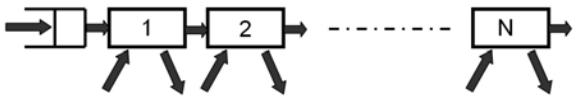

Figure 1. FREEWAY WITH N SECTIONS.

Symbol	Name	Units
F_i	maximum flow (capacity) of section i	veh/period
v_i	free flow speed of section i	section/period
w_i	congestion wave speed of section i	section/period
n_i^c	critical density of section i	veh/section
n_i^J	jam density of section i	veh/section
$f_i(k)$	flow from section i to $i+1$ at period k	veh/period
$s_i(k), r_i(k)$	off-ramp, on-ramp flow in section i at period k	veh/period
$n_i(k)$	number of vehicles in section i at period k	veh/section
$Q(k)$	number of vehicles in the input queue to section 1 at period k	veh
$f_{in}(k)$	input flow at upstream queue at period k	veh/period

Table 1. Model Variables and Parameters

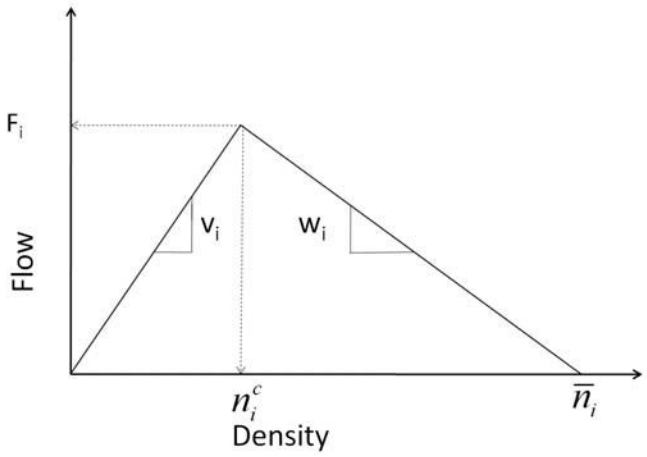

Figure 2. FUNDAMENTAL DIAGRAM OF SECTION i.

The ACTM is a space and time discretization of the Lighthill-Whitham-Richards (LWR) equation [12], [13] and it can be formulated as a continuous time spatially discretized model, as pre-

sented in [11]. The boundary conditions are specified as free flow at the downstream boundary and the upstream flow is fed to the freeway through a queue. Table 1 lists the model variables and parameters. The ACTM can be described by the following equations.

$$\dot{n}_i(k) = f_{i-1}(k) - f_i(k) + r_i(k) - s_i(k), \quad 1 \le i \le N \tag{1}$$

$$f_i(k) = \min(v_i n_i(k) - s_i(k), w_{i+1}[n^J_{i+1} - n_{i+1}(k)], F_i) \quad 1 \le i < N \tag{2}$$

$$f_N(k) = \min(v_N n_N(k) - s_N(k), F_N) \tag{3}$$

$$f_0(k) = \min(w_1[n^J_1 - n_1(k)], Q(k) + f_{in}(k)) \tag{4}$$

$$Q(k+1) = Q(k) + f_{in}(k) - f_0(k) \tag{5}$$

where i is the cell index and k is the continuous time index. A cell i is said to be in free flow if its corresponding discharge flow $f_i(k)$ satisfies

$$v_i n_i(k) - s_i(k) < \min[w_{i+1}[n^J_{i+1} - n_{i+1}(k)], F_i] \tag{6}$$

and it is in congestion if the inequality above is violated. Hence, the system essentially is a switching mode system with congested and free flow modes for each cell.

After the model is calibrated, the unavailable ramp flows are reconstructed using an iterative learning algorithm which matches the mainline flows by fitting artificial ramp flows at specified locations. The imputation is carried out sequentially for each section, starting from the most upstream. For estimation of ramps in section i, only the immediate upstream section $i-1$ and the immediate downstream section $i+1$ are considered. In the following, the upstream section is specified with the subscript up and the downstream section is specified by dn. Figure 3 shows the parameters and measurements used for imputation of ramp flows in section i. The upstream boundary conditions include the upstream density, fundamental diagram parameters and the off-ramp flow $s_{i,up}$. Since all the parameters and variables carry the subscript i, for clarity, we drop it in the following equations. For

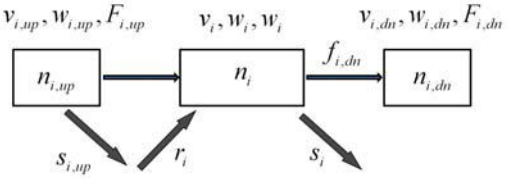

Figure 3. Imputation Parameters and Cell Definitions

each section, the imputation procedure assumes initial estimates for the ramp parameter functions $\hat{c}_r$ and $\hat{c}_s$. These estimates are then adapted so that the model calculated densities match the density profile measured by the vehicle detector station. The model variables and the estimates are denoted by a hat accent ($\hat{}$) and the residuals by a tilde accent ($\tilde{}$). The true values are represented without any accent.

It is assumed that the density and ramp flow profiles are 24 hour periodic, and the on-ramp and off-ramp flows are represented as a convolution of a kernel with a constant periodic ramp flow parameter vector:

$$r(k) = \int_0^T K_r(\tau,k) c_r(\tau) d\tau, \quad s(k) = \int_0^T K_s(\tau,k) c_s(\tau) d\tau \tag{7}$$

In equation (7), $K_r(\tau,k)$ and $K_s(\tau,k)$ represent periodic, time dependent kernel functions with a period of 24 hours. A typical kernel function would be an impulse or a gaussian window centered at time k.

The four modes considered by the imputation algorithm are: 1)P-F: Plant in Free Flow, 2)P-C: Plant in congestion, 3)M-F: Model in Free Flow, 4)M-C: Model in Congestion. These modes are determined by equation (6). The mode dependent adaptation laws for the parameters at each step are given by:

(a) P-F , M-F (plant and model are both in free-flow downstream)

$$\begin{aligned} \dot{\hat{c}}_r(\tau,k) &= G_1 K_r(\tau,k)\tilde{n}(k) \\ \dot{\hat{c}}_s(\tau,k) &= -G_2 K_s(\tau,k)\tilde{f}_{dn}(k) \end{aligned} \tag{8}$$

(b) P-C , M-C (plant and model are both in congestion downstream)

$$\begin{aligned} \dot{\hat{c}}_r(\tau,k) &= G_1 K_r(\tau,k)\tilde{n}(k) \\ \dot{\hat{c}}_s(\tau,k) &= -G_1 K_s(\tau,k)\tilde{n}(k) \end{aligned} \tag{9}$$

(c) P-C , M-F (plant is in congestion and model is in free flow downstream)

$$\begin{aligned} &Case(i) \qquad \tilde{n}(k) > 0 \\ &\dot{\hat{c}}_r(\tau,k) = G_1 K_r(\tau,k)\tilde{n}(k) \\ &\dot{\hat{c}}_s(\tau,k) = -G_1 K_s(\tau,k)\tilde{n}(k) - G_2 K_s(\tau,k)\frac{\tilde{f}_{dn}(k) + |\tilde{f}_{dn}(k)|}{2} \end{aligned}$$

$$\begin{aligned} &Case(ii) \qquad \tilde{n}(k) \le 0 \\ &\dot{\hat{c}}_r(\tau,k) = G_1 K_r(\tau,k)\tilde{n}(k) \\ &\dot{\hat{c}}_s(\tau,k) = -G_2 K_s(\tau,k)\tilde{f}_{dn}(k) \end{aligned} \tag{10}$$

(d) P-F , M-C (plant is in free flow and model is in congestion

downstream)

$$
\begin{aligned}
&Case(i) \qquad \tilde{n}(k) < 0 \\
&\dot{\hat{c}}_r(\tau,k) = G_1 K_r(\tau,k)\tilde{n}(k) \\
&\dot{\hat{c}}_s(\tau,k) = -G_1 K_s(\tau,k)\tilde{n}(k) - G_2 K_s(\tau,k)\tilde{f}_{dn}(k) \\
&Case(ii) \qquad \tilde{n}(k) \geq 0 \\
&\dot{\hat{c}}_r(\tau,k) = G_1 K_r(\tau,k)\tilde{n}(k) \\
&\dot{\hat{c}}_s(\tau,k) = -G_2 K_s(\tau,k)\tilde{f}_{dn}(k)
\end{aligned} \tag{11}
$$

where G's are user defined positive gains.

The model density update at each steps is given by

$$\tilde{n}(k) = n(k) - \hat{n}(k) \tag{12}$$

$$\dot{\hat{n}}(k) = \hat{f}_u - \hat{f}_d + \hat{r}(k) - \hat{s}(k) - a\tilde{n}(k) \tag{13}$$

$$\hat{f}_u = min(n_{up}(k)v_{up} - s_{up}(k), F_{up}, w(n^J - \hat{n}(k))) \tag{14}$$

$$\hat{f}_d = min(\hat{n}(k)v - \hat{s}(k), \bar{w}_{dn}(k)(n^J_{dn} - n_{dn}(k))) \tag{15}$$

$$\tilde{f}_{dn}(k) = f_{dn}(k) - (n(k)v - \hat{s}(k)) \tag{16}$$

where $\bar{w}_{dn}(k) = min\left(\frac{F}{n^J_{dn} - n_{dn}(k)}, w\right)$ is introduced in order to absorb the capacity flow into the congestion mode and the parameter a in (13) is chosen so as to make the error equations asymptotically stable. While the parameter and model density update equations are given in continuous time, the model is implemented in discrete time with a small time step and small gains, so that the imputation procedure as well as the model are stable. The adaptation is carried out for the entire density profile multiple times, so as to reduce the 24-hour 'residuals' $\sum_k |n(k) - \hat{n}(k)|$ and $\sum_k |f_{dn}(k) - \hat{f}_{dn}(k)|$. This procedure is repeated until either both the residuals become small (eg. $< 0.5\% \quad of \quad \sum_k n(k)$ and $< 0.5\% \quad of \quad \sum_k f_{dn}(k)$) or the residuals do not improve (eg. change of errors of $< 0.5\%$ of $\sum_k n(k)$ and $< 0.5\%$ of $\sum_k f_{dn}(k)$ across iterations)

3 AUTOMATED FAULT DETECTION AND EXCLUSION

In the modeling procedure outlined in section 2 the identification of faulty mainline detectors, when carried out manually, is the most time-consuming step of the procedure. Therefore, an automated procedure based on the evaluation of residuals between the measured and simulated densities and flows is introduced to determine to what degree the mainline measurements are corrupted. Figure 4 shows the block diagram of this framework. An important point to make here is that the model evaluation and unknown input estimation are carried through off-line, once the freeway data is available for the whole day. For this reason, the fault detection module also works off-line and evaluates residuals for the whole day rather than monitoring them in real time.

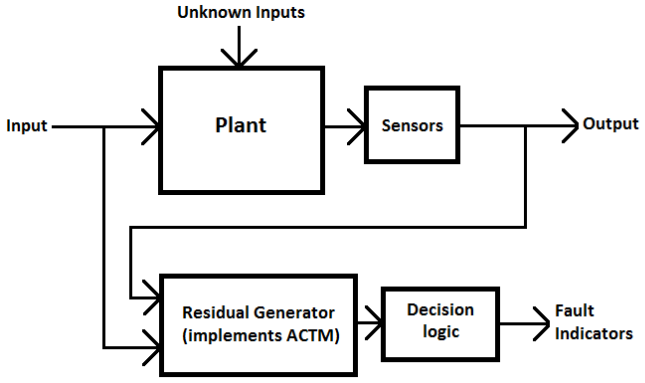

Figure 4. Fault Detection Framework

The placement of detectors on California freeways follows the simple rule of placing detectors just upstream of on-ramps and downstream of off-ramps. As a result, the density measurements associated with each cell carry a certain bias, due to the fact that they actually measure the density just upstream of the cell and fail to include the effect of ramp flows. Figure 5 gives the basic configuration of the model and the location of detectors with respect to the model. In this figure, the cells are enumerated as 1 and 2, the ramp flows are indicated by the arrows below as r and s and the measurements f (Flow) and n (density) are taken at the locations indicated by the circles. Since density is the essential state of the model on which both the imputation and the simulations are based, this bias has a significant effect on the accuracy of the model. This phenomenon constitutes the basic reason for a model based fault detection algorithm.

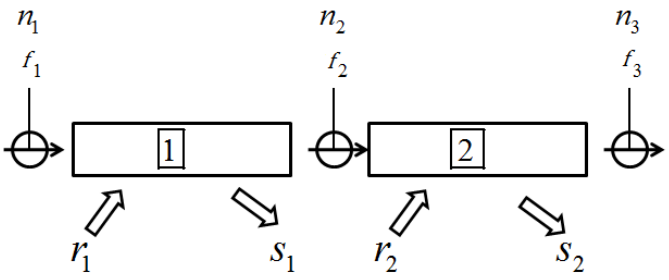

Figure 5. Basic configuration and Location of Detectors

The first step in devising the algorithm was to create artificial faults in known locations on the freeway and analyze where these faults manifest themselves after the missing ramps are imputed and the model is simulated using the available boundary condition data. A convenient consequence of using the ACTM is that

the fault in the measurements of a cell only affects the cell itself, and the two cells adjacent to it, but not the other cells. On the other hand, a consequence of having unknown inputs that need to be imputed causes the fault signatures to be dependent on the specific ramp geometry of the analyzed section. As an example, consider 3 successive cells, all of which have both an on-ramp and an off-ramp and none of the ramp data is available (i.e. they are all to be imputed). This configuration is depicted in figure 6. We inject bias terms, ϕ and ψ, respectively, in the flow and density measurements just upstream of cell 2, which the model assigns as the flow entering cell 2 and density of cell 2, respectively. To conform with the model definition in section 1, we denote the flow measured at this location f_1 whereas the density measurement is named n_2 but in reality these two measurements belong to the same vds. Since nothing is assumed about the artificial error terms, they can, in theory, be any function of time.

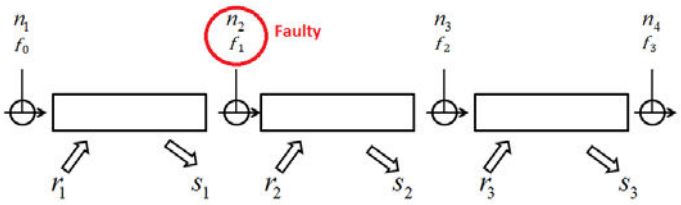

Figure 6. Example Ramp Configuration

We have:

$$f_1^m = f_1^T + \phi_1$$
$$n_2^m = n_2^T + \psi_2$$

where superscript m stands for measured and T stands for truth. In the presence of these artificial faults, the plant, model and residual dynamics in free flow evolve according to the following equations:

Plant:

$$\dot{n}_1 = -v_1 n_1 + f_0 + r_1$$
$$\dot{n}_2 = -v_2 n_2 + v_1 n_1 - s_1 + r_2$$
$$\dot{n}_3 = -v_3 n_3 + v_2 n_2 - s_2 + r_3$$

Model:

$$\dot{\hat{n}}_1 = -v_1 \hat{n}_1 + f_0^m + \hat{r}_1$$
$$\dot{\hat{n}}_2 = -v_2 \hat{n}_2 + v_1 \hat{n}_1 - \hat{s}_1 + \hat{r}_2$$
$$\dot{\hat{n}}_3 = -v_3 \hat{n}_3 + v_2 \hat{n}_2 - \hat{s}_2 + \hat{r}_3$$

Residuals:

$$\dot{\tilde{n}}_1 = -v_1 \tilde{n}_1 + \tilde{r}_1$$
$$\dot{\tilde{n}}_2 = -v_2 \hat{n}_2 + v_2 \psi_2 + \dot{\psi}_2 + \tilde{r}_2 - \phi_1$$
$$\dot{\tilde{n}}_3 = -v_3 \tilde{n}_3 + \tilde{r}_3$$

where the hat accents are reserved for the model and the tilde accents are reserved for residuals and in the last part, we have used

$$v_1 \hat{n}_1 - \hat{s}_1 = f_1^m$$
$$v_2 \hat{n}_2 - \hat{s}_2 = f_2$$

On the other hand, during congestion, the dynamics evolve according to the equations below:

Plant:

$$\dot{n}_3 = w_3(n_3^J - n_3) - f_3 + r_3 - s_3 \text{ (not affected)}$$
$$\dot{n}_2 = w_2(n_2^J - n_2) - w_3(n_3^J - n_3) + r_2 - s_2$$
$$\dot{n}_1 = f_0^m - w_2(n_2^J - n_2) + r_1 - s_1$$

Model:

$$\dot{\hat{n}}_2 = w_2(n_2^J - \hat{n}_2) - f_2 + \hat{r}_2 - \hat{s}_2$$
$$\hat{n}_1 = f_0 - w_2(n_2^J - \hat{n}_2) + \hat{r}_1 - \hat{s}_1$$

Residuals:

$$\tilde{n}_2 = -\tilde{n}_2 w_2 + w_2 \psi_2 + \dot{\psi}_2 + \tilde{d}_2$$
$$\tilde{n}_1 = \tilde{n}_2 w_2 - w_2 \psi_2 + \tilde{d}_1$$

where $d_i = r_i - s_i$ is the total demand.

To simplify the analysis, only the two cases where the middle cell is either in free flow or in congestion are considered and it is assumed that the adjacent cell affected by the middle cell (which is the upstream cell when the middle cell is in congestion and the downstream cell when it is in free flow) is in the same mode as the middle cell. This does not compromise the algorithm's ability to detect faults since the instances where two successive cells are on different flow modes are transient and do not prevail for extended periods of time. After the imputation algorithm is applied, the model profiles converge to the following values during free flow and congestion respectively:

Free Flow:

$$\begin{aligned}
&\hat{n}_1 \rightarrow n_1 \\
&\hat{n}_2 \rightarrow n_2^m (= n_2^T + \psi_2) \\
&\hat{f}_1 \rightarrow f_1^m (= f_1^T + \phi_1) \\
&\hat{d}_1 \rightarrow d_1^T + \phi_1 \\
&\hat{d}_2 \rightarrow d_2^T - \phi_1 + \psi_2
\end{aligned}$$

Congestion:

$$\begin{aligned}
&\hat{n}_1 \rightarrow n_1 \\
&\hat{n}_2 \rightarrow n_2^m (= n_2^T + \psi_2) \\
&\hat{f}_1 \rightarrow f_1^m - \phi_1 - w_2\psi_2 \\
&\hat{d}_1 \rightarrow d_1^T - w_2\psi_2 \\
&\hat{d}_2 \rightarrow d_2^T + w_2\psi_2 + \psi_2
\end{aligned}$$

It is seen that the faults manifest themselves in two distinct ways for this particular configuration of unknown ramp flows: 1) The measured and simulated flows discharged by cell 1 do not match during congestion, 2) The estimated total demands for cells 1 and 2 show a significant instant change when the mode switches from free flow to congestion.

There are 5 possible fault signatures that show up as residuals between the model and plant:

1. Density mismatch during free flow
2. Density mismatch during congestion
3. Flow mismatch during free flow
4. Flow mismatch during congestion
5. "Jump" in estimated demand when there is a switch in flow conditions

Since the fault signatures are dependent on which ramps are to be estimated in a cell triplet, they were evaluated for all 64 possibilities of ramp configurations, similar to the example given above. The given example happens to be case 64, whereas case 1 is a triplet of cells with no ramps at all. 4 modes of systematic fault were considered:

1. Positive Bias in Density
2. Negative Bias in Density
3. Positive Bias in Flow
4. Negative Bias in Flow

If the middle cell in a three cell cascade is subject to any of the above failure modes, a unique combination of the 5 signatures occur in all the three cells. In the given example this combination is "Signature 4 in Cell 1 and Signature 5 in Cells 1 and 2", which are due to "Positive Bias in Density" and "Positive Bias in Flow".

The automated algorithm is essentially a look-up-table logic that takes the cells on the freeway in sets of 3, determines the specific ramp configuration and checks whether the density and flow residuals show characteristics pertaining to any of the failure modes listed above. Section 4 presents an example of a real freeway section with a different ramp configuration and fault signatures than the ones presented in this section.

Several subtleties must be addressed here:

Effect of Ramp Flows: When ramp flows are available and do not need to be estimated, the imputation algorithm does not have the freedom to feed estimated ramp flows to match the measurements. As a result, knowing the flows of a ramp has the same effect on the fault detection algorithm as if the ramp did not exist at all. This, of course, inherently assumes that ramp flow measurements are error-free. Although this assumption is too optimistic, once the algorithm flags the inconsistent mainline detector, the user can still decide whether the error is actually due to the ramp flow and discard the ramp flow data rather than the mainline data, thus supplying the imputation algorithm with an additional degree of freedom. The algorithm will consequently classify the geometry differently and evaluate the quality of the mainline data under the new ramp configuration.

Thresholds: As mentioned earlier, most of the detectors are subject to varying levels of measurement bias, especially in density. Since as a rule of thumb, the total model errors are aimed to be brought down to below 10%, the algorithm deems a mismatch as a valid signature if the absolute error is more than 10% of the maximum value of the quantity under question during the given day.

Faults occurring in successive cells: When successive cells have faulty measurements, the signatures can superpose and / or overlap. In the algorithm, the signatures for a certain mode of failure are sufficient conditions for raising a flag

and do not have to be exclusive. If, for instance, a set of cells shows Signatures 1,3 in cell 1, Signatures 1,2,3,4 and 5 in cell 2 and Signature 1 in cell 3, a flag is raised for the combination 1,3 in cell 1; 2,4 and 5 in cell 2 and none in cell 3, if there exists a failure mode that is explained by these signatures for the specific ramp geometry. Hence, successive faulty detectors are also flagged accurately by the algorithm.

Unobservable Faults: It is obvious that some signatures only appear when the section under question gets congested during the day. If this is not the case on a given day, the fault, even if it exists, is not observable and since it doesn't affect the model calibration by causing an undesired residual, it can be ignored.

Effect of Fundamental Diagram Parameter Errors: As mentioned in the introduction, the fundamental diagram parameters are calibrated based on many days' data. Since the imputation is carried through on a specific days' mainline data, if for instance there is a significant capacity drop at a freeway section due to an incident, that section may produce significant residuals and may be flagged by the algorithm as faulty.

4 RESULTS

After it has been experimentally established that bias in the flow or density measurements of a given cell has specific effects on the imputed ramp flows and consequently on the simulated flows, and densities of the cell and the adjacent cells upstream and downstream, an automated algorithm was deployed to determine the erroneous mainline detectors. The algorithm was tested on a previously calibrated 23 mile section of Interstate 210W and was able to automatically flag the bad detectors which were originally picked out by manual inspection. The exclusion of 7 poor performance detectors from the 30 cell model, reduces the number of cells to 23 but also reduces the total density errors along the freeway section to around 4.8% from 9.6% and flow errors to around 9% from 14%.

An example section is shown in figure 7, which is a section from Westbound Interstate 210 in Southern California. The diagrams belong to cell 7 in the figure and the horizontal axis is the time of day whereas the vertical axes are density (in units of vehicles per mile) and flow (in units of vehicles per hour), respectively from left to right. The diagram on the left shows the simulated (nhat) and measured (n true) density profiles throughout the day along with the critical density for the section (horizontal line), and the diagram on the right provides simulated (fhat) vs. measured (f true) flows. It is clear that there is significant difference between measurement and simulation during congestion (i.e. when density is above its critical value). The data is aggregated over 5

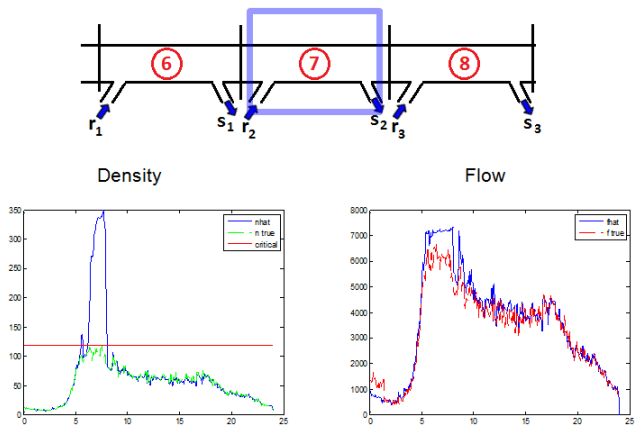

Figure 7. An Example Section with Faulty Measurements

minute intervals by PeMS. Here, the ramp flows r_1, s_1, r_2, s_2, and r_3 are measured and s_3 is imputed. The fault signatures corresponding to this specific geometry are given below (since we readily know that the faulty detector is the one corresponding to cell 8 in this case, we present below the case where cell 8 is the middle detector in a triplet cascade)

Free Flow:

$$\hat{n}_7 \rightarrow n_7$$
$$\hat{n}_8 \rightarrow n_8^m (= n_8^T + \psi_8)$$
$$\hat{f}_7 \rightarrow f_7^m$$

Congestion:

$$\hat{n}_7 \rightarrow n_7 + \int w_8 \psi_8$$
$$\hat{n}_8 \rightarrow n_8^m (= n_8^T + \psi_8)$$
$$\hat{f}_7 \rightarrow f_7^m + w_2 \psi_2$$

In other words, the algorithm tested this section for fault mode 1, "Positive Bias in Density", and the "Density mismatch during congestion" and "Flow Mismatch during congestion" signatures caused the algorithm to flag this location as faulty. Both signatures are visible in figure 7.

Once the faulty detectors are identified, the data they provide is discarded, along with the cell it belongs to, creating a so-called mega-cell. Cell 7 becomes the mega-cell in this case, as depicted in figure 8. The ramps of the joined cells are also assumed to be joined to a single on-ramp and off-ramp for consistency with the model, i.e. r_2 in figure 8 is $r_2 + r_3$ in truth and s_3 is $s_2 + s_3$.

This reduces the residual between simulated and measured flow and density values along with the number of cells in the model. Therefore, there is a trade-off between the geometric accuracy and the numerical accuracy of the model. The results of removing the faulty sections, which in this example happens to be the cell numbered 8, are also shown in figure 8.

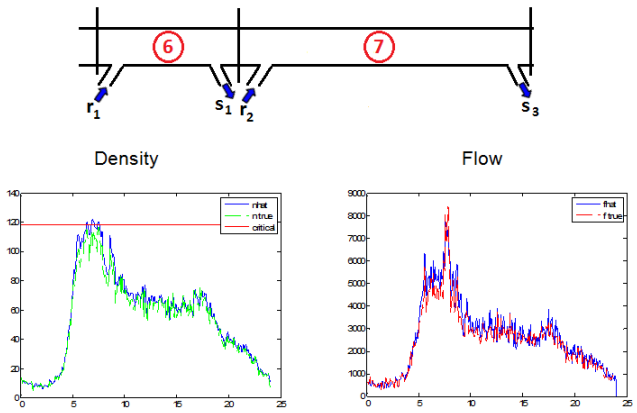

Figure 8. The Example Section after discarding the faulty mainline detector

5 CONCLUSION

An automated methodology based on residual analysis to detect faulty measurements along a freeway is introduced. The algorithm is a look-up-table logic which evaluates the residuals between the model and the plant in accordance with the freeway geometry and raises a flag if all signatures of a certain type of fault are present at a given section. Exclusion rather than correction is preferred since the exact estimation of fault, in general, is not possible due to unknown inputs. In theory, if all ramp inputs were known, the bias in the measurements can be estimated. However, out of the 4 freeways that were modeled by the TOPl project, namely I210, I80, I880 and I680, only I210 had monitored ramp data available, and even in that case most of the ramp data was reported to be bad by the built-in algorithm in the PeMS repository and had to be imputed. If ramp data and accurate density data become available, further advancements can be made to actually estimate the faults rather than just to detect them and a model-based scheme can be deployed even in real time.

6 ACKNOWLEDGEMENTS

This work is supported through the NSF CDI Grant 0941326. The contents of this paper reflect the views of the author and not necessarily the official views or policy of the National Science Foundation. The authors would like to thank the TOPl group for the concerted effort in developing the ideas and software tools that made this study possible. We are also grateful for the insightful comments and suggestions by the anonymous reviewers.

REFERENCES

[1] C. Daganzo, "The cell transmission model: A dynamic representation of highway traffic consistent with the hydrodynamic theory," *Transportation Research, Part B*, vol. 28, no. 4, pp. 269–287, 1994.

[2] G. Gomes and R. Horowitz, "Optimal freeway ramp metering using the asymmetric cell transmission model," *Transportation Research, Part C*, vol. 14, no. 4, pp. 244–262, 2006.

[3] "Topl website." http://gateway.path.berkeley.edu/topl/.

[4] "PeMS website." http://pems.eecs.berkeley.edu.

[5] C. Chen, J. Kwon, J. Rice, A. Skabardonis, and P. Varaiya, "Detecting errors and imputing missing data for single loop surveillance systems," in *Transportation Research Record*, vol. 1855, (Washington DC), pp. 160–167, TRB, National Research Council, 2003.

[6] J. Kwon, C. Chen, and P. Varaiya, "Statistical methods for detecting spatial configuration errors in traffic surveillance," *Transportation Research Record*, vol. 1870, pp. 124–132, 2005.

[7] R. Rajagopal, X. Nguyen, S. C. Ergen and P. Varaiya, "Distributed online simultaneous fault detection for multiple sensors," in *Proceedings of the 2008 Intl. Conf. on Information Processing in Sensor Networks (IPSN 2008)*, 2008.

[8] C. Claudel and A. Bayen, "Minimal error certificates for detection of faulty sensors using convex optimization," 2009. Allerton Conference on Communication and Control, Allerton, IL.

[9] J. Huper and et al., "Macroscopic modeling and simulation of freeway traffic flow," 2009. 12th IFAC Symposium on Control in Transportation Systems.

[10] G. Dervisoglu, G. Gomes, J. Kwon, R. Horowitz, and P. Varaiya, "Automatic calibration of the fundamental diagram and empirical observations on capacity," Transportation Research Board, 88th Annual Meeting, 2009.

[11] A. Muralidharan and R. Horowitz, "Imputation of ramp flow data using the asymmetric cell transmission traffic flow model," ASME Dynamic Systems and Control Conference, 2009.

[12] M. Lighthill and G. Whitham, "On kinematic waves I: Flow movement in long rivers. II: A theory of traffic flow on long crowded roads," *Proc. Royal Society of London, Part A*, vol. 229, no. 1178, pp. 281–345, 1955.

[13] P. Richards, "Shock waves on the highway," *Operations Research*, vol. 4, no. 1, pp. 42–51, 1956.